HAPAN: Support Tool for Practicing Regional Anesthesia in Peripheral Nerves

J. A. Hernández-Muriel(✉), J. C. Mejía-Hernández, J. D. Echeverry-Correa, A. A. Orozco, and D. Cárdenas-Peña

Automatic Research Group, Faculty of Engineerings, Universidad Tecnológica de Pereira, Pereira, Colombia
j.hernandez12@utp.edu.co

Abstract. Ultrasound (US) medical imaging rises as a technique used to visualize nerve structures, among other applications. It has been used, typically, as a tool for assisting in the practice of peripheral nerve anesthesia. Due to its non-invasive nature, US may reduce the risk of injury to medical patients during surgical procedures. Despite its usefulness, it is challenging for anesthesiologists to perform the anesthesia process, mainly due to the presence of speckle and acoustic multiplicative noise, significantly degrading the image quality. Besides, the lack of homogeneity in the imaged structures disorients the anesthesiologist in the effective localization of the nerve structure. In this paper, we present the design and implementation of the software toolkit HAPAN (HAPAN is a Spanish acronym for ***H****erramienta de* ***A****sistencia para la* ***P****ráctica de* ***A****nestesia en* ***N****ervios periféricos*-Assistance tool for the anesthesia of peripheral nerves.), developed in MATLAB, for the segmentation of different peripheral nerves in ultrasound images. HAPAN includes algorithms for automatic nerve segmentation based on appearance shape models, and image resolution enhancement.

Keywords: Peripheral nerves · Regional anesthesia · Support tool

1 Introduction

Medical ultrasound (US) imaging stands as a technology widely used by anesthesiologists for the localization of nerves structures [14]. Despite being the standard tool for peripheral nerve blocking, the US strongly suffers from multiplicative acoustic noise and lack of structure homogeneity [16]. To deal with above issues, researches focus on the automatic segmentation of US including fetal catches [1,8], blood vessels [10,15], and pathological tissue [11,19]. In general, the approaches of US segmentation are grouped into statistical approaches [9,13], superpixel or patch-based approaches [2,18], and texture and classification approaches [7,12].

Nonetheless, there are few relevant approaches for peripheral nerve segmentation that provide on-line assistance to the anesthesiologists. Some of them

J. M. Ferrández Vicente et al. (Eds.): IWINAC 2019, LNCS 11486, pp. 130–137, 2019.
https://doi.org/10.1007/978-3-030-19591-5_14

include are clustering algorithms [4], Bayesian shape models [3]; and Gaussian processes [5,6]. Despite reporting promising results, most of the works only test small US collections. Therefore, there is a need for tools allowing anesthesiologist visualization, validation, and analysis of automatic US processing.

This paper presents the design and development of software for the automatic segmentation of ultrasound images, termed HAPAN. HAPAN includes conventional segmentation and appearance and shape models as user alternatives. Besides, HAPAN as a support software deploys complementary tools ranging from digital filters to image resolution enhancement algorithms, developed to facilitate the visualization and localization of the nerve in ultrasound images.

The rest of the article is organized as follows. Section 2 provides a detailed analysis of materials and methods. Section 3 discusses the experimental results. Section 4 presents the concluding remarks and future research directions.

2 Materials and Methods

2.1 Database

The database used for building the HAPAN Software contains a collection of approximately 200 ultrasound images. Two peripheral nerves from 6 different patients were captured. Ultrasonic images were obtained by an acquisition system consisting of the combination of a portable NanoMaxx SONOSITE ultrasound system with a video converter (EASYCAP). The ultrasound system is used to acquire the image of the nerve to study by means of an ultrasonic transducer, and the EASYCAP system allows the scanner to communicate directly with the computer in which the processing will be performed. Any scanner that has similar characteristics to the one used in HAPAN could be compatible with the software. Acquired images go through a pre-processing stage which performs a series of adjustments in order to enhance the quality of the image.

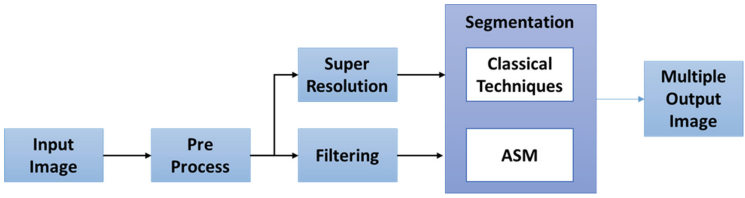

Fig. 1. HAPAN software structure.

2.2 Software Development

HAPAN's interface is comprised of two processing methods and two processing tools, which can be used at any time. The software structure can be seen in Fig. 1. Hapan allows many actions, Zoom In, Zoom Out, Open Images or Projects, Save Images or Projects, Helps and Captures Images directly from the scanner. Figure 2 shows the application interface in which the user can appreciate the different images generated by the software.

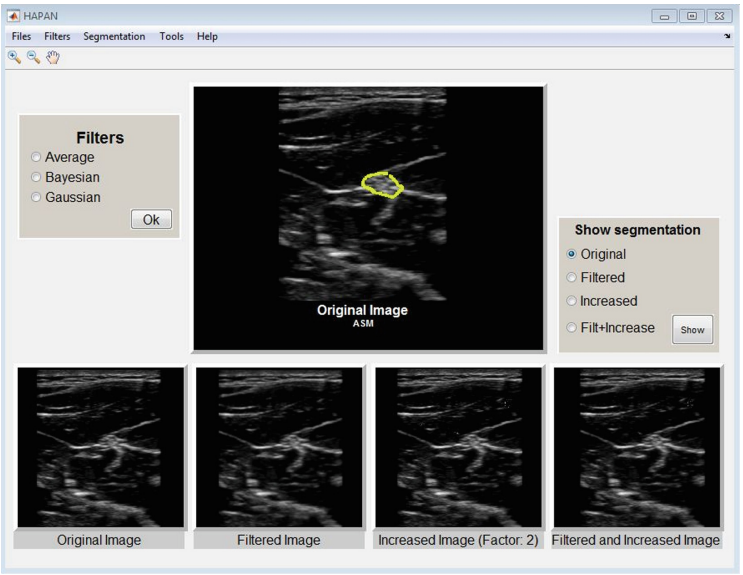

Fig. 2. Software interface for processing ultrasonic images.

2.3 Methodologies

Two different methodologies were used in the segmentation of the peripheral nerve: Classical Techniques and Appearance and Shape Models.

Classical Techniques. This methodology is based on the classical techniques of digital image processing, such as identifying edges, thresholding, dilation, erosion, opening, and closing areas. These techniques are used iteratively to identify the nerve structure in the ultrasound image.

Appearance and Shape Models. It is a semiautomatic method, which can be trained to learn the different forms of nerve structures that can be found in the database. This model requires, as an initial step, that the user locates an ellipsoidal contour on the region containing the nerve structure. Then, the algorithm adjust the contour to the nerve structure in the image. One of the drawbacks of this method is that it requires that the initial region (the ellipsoidal contour placed by the user) contains the nerve structure. If this constraint is not fulfilled, the algorithm would perform the segmentation to a different region of the image.

2.4 Tools

The HAPAN's tools are used to improve the quality of the image and therefore to obtain a more accurate segmentation of the nerve structure. The user is allowed to change the parameters of these tools.

Image Filtering. When an echography is acquired by the scanner, the image is commonly corrupted either by Speckle noise, random variations in intensity, poor contrast or illumination variations as a result of changes in gain or depth of the scanner. The segmentation algorithms used in HAPAN were designed to tackle these effects to some extent. In some cases, these algorithms do not accomplish this goal; however, in those cases an improved segmentation is possible by using image filtering techniques. HAPAN includes the following filters:

- Average filter: This is a two dimensional digital filter which averages the neighborhood of pixels. The default size for this filter is 3×3 pixels.
- Gaussian: A Gaussian low pass digital filter with a symmetric rotation, with standard deviation sigma. The default size of this filter is 3×3 pixels and the default sigma's value is 0,5.
- Bayesian: A Bayesian framework is used to adapt the Non Local (NL) means filter for removing speckle noise in ultrasound images. This algorithm introduces the Pearson distance as a relevant measure for region comparison [20].

Super-Resolution. This tool allows to create a new image, based on the original, performing an increase of the resolution by an user-adjustable factor (2, 3, 4, and so on). The objective is to generate a high-resolution image from a single low-resolution image without any external training set. It uses a framework for both magnification and de-blurring using only the original low-resolution image and its blurred version. In this method, each pixel is predicted by its neighbors through a Gaussian process regression [17].

3 Experimental Results and Discussion

3.1 System Efficiency

The leftmost columns in Table 1 shows the results of the performance of the methodologies implemented in HAPAN in terms of computational consumption (CC) for each of the techniques used during the segmentation process. The test was performed on a Intel Core i3 with 4 GB RAM. The nomenclature used in Table 1 is **CT:** Classical Techniques, **ASM:** Appearance and Shape Models, **AF:** Average Filter, **BF:** Bayesian Filter, **GF:** Gaussian Filter, **IR:** Increased Resolution.

The results show that the computational consumption is considerably low when the user do not use any of the additional tools provided by the software. The results also show that the most efficient methodology (in terms of CC) are the classical techniques. This efficiency is due basically to the fact that its processes and algorithms have a low computational cost. The tools with the lowest cost (in terms of time) are IR[1] and BF.

[1] The average execution time of the algorithm with a $\times 2$ factor is about one hour.

3.2 Validation

This software has been tested using a database composed of ultrasound images. These images have been manually labeled by an anesthesiologist. The performance of the system was evaluated using two parameters: dice similarity coefficient and F1 score. These metrics have been computed for measuring the efficiency of both segmentation methods and the additional software tools.

Dice Similarity Coefficient (DSC). DSC is a commonly used metric for evaluating the accuracy of automated or semi-automated segmentation methods. In this work, DSC has been used as a statistical validation metric to evaluate the similarity between two samples (the labels created by the anesthesiologist and the labels provided by HAPAN).

F1 Score. F1 score is a measure of a test's accuracy. It considers both the precision (the number of true positive results divided by the number of all positive results) and the recall (the number of true positive results divided by the number of true positive plus false negative results) of the test. The F1 score can be interpreted as a weighted average of the precision and recall, where an F1 score reaches its best value at 1 and worst at 0.

3.3 Practical Results and Discussion

This section presents the results obtained by HAPAN in the segmentation of the ultrasound images of the database. Figure 3 shows an example of an ASM segmentation process by using an image of a Median nerve. Figure 3(a) shows the original image without segmentation. Figure 3(b) presents the original image after the segmentation process. Figure 3(c) shows the image after both filtering and segmentation processes. Figure 3(d) illustrates the segmented image by taking as input an increased resolution version of the original image. Figure 3(e) shows the image obtained by increasing the resolution, filtering and applying the segmentation process on the original image.

The rightmost columns in Table 1 show the global performance results of the HAPAN software. These results were obtained by processing all the ultrasound images of the database. Both methodologies and all the additional tools were evaluated. Remind that the database was previously described in Sect. 2.1.

Results in Table 1 show that the best segmentation performance, using DSC, can be obtained in the Cubital nerve ($0{,}672 \pm 0{,}04$). This result is achieved using a Bayesian filter in the preprocessing stage and the ASM methodology for the segmentation process. However, it must be noticed that this performance is not statistically significant when compared to the same procedure in the Median nerve ($0{,}604 \pm 0{,}047$).

When using the F1 score for comparing the effectiveness of the methodologies, results show that the best performance is achieved in the Median nerve ($0{,}573 \pm 0{,}042$) by means of an Average filter and Classical techniques. This result improves significantly the performance obtained in the Cubital nerve by the same techniques.

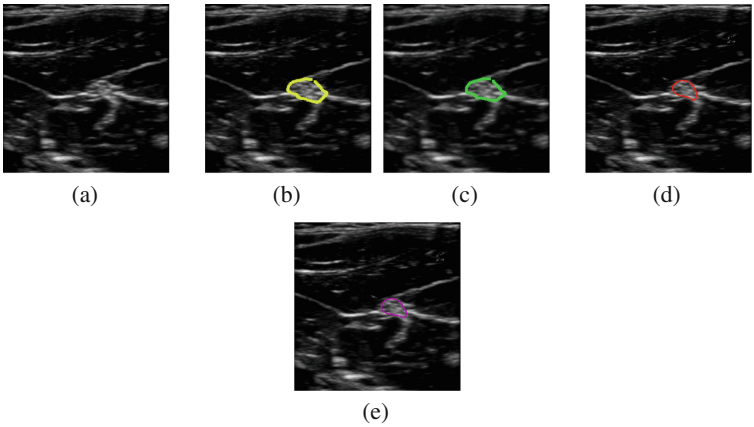

Fig. 3. Example of a practical result obtained with HAPAN. (a) Original image. (b) Original image segmented using ASM. (c) Filtered image and segmented using ASM. (d) Increased resolution (×2 factor) and segmented image using ASM. (e) Increased resolution (×2 factor), filtered and segmented image using ASM.

Table 1. Global performance results of the HAPAN software

Process	Median nerve	Cubital nerve	Median nerve		Cubital nerve	
	Time (s)	Time (s)	Dice	F1 score	Dice	F1 score
CT	0,330 ± 0,003	0,328 ± 0,007	0,647 ± 0,041	0,567 ± 0,041	0,519 ± 0,063	0,437 ± 0,065
CT+AF	0,336 ± 0,003	0,380 ± 0,019	**0,663 ± 0,041**	**0,573 ± 0,042**	0,532 ± 0,062	0,452 ± 0,064
CT+BF	14,88 ± 0,234	15,36 ± 0,521	0,653 ± 0,041	0,571 ± 0,041	0,565 ± 0,053	0,487 ± 0,060
CT+GF	0,364 ± 0,009	0,368 ± 0,015	0,653 ± 0,041	0,570 ± 0,041	0,539 ± 0,059	0,455 ± 0,062
CT+IR	0,521 ± 0,022	0,973 ± 0,035	0,577 ± 0,030	0,447 ± 0,034	0,479 ± 0,073	0,425 ± 0,055
CT+AF+IR	0,514 ± 0,021	0,945 ± 0,032	0,581 ± 0,031	0,450 ± 0,035	0,491 ± 0,070	0,439 ± 0,052
CT+BF+IR	26,51 ± 1,131	44,69 ± 1,934	0,579 ± 0,030	0,447 ± 0,034	0,493 ± 0,071	0,426 ± 0,055
CT+GF+IR	0,640 ± 0,038	0,895 ± 0,026	0,578 ± 0,031	0,447 ± 0,034	0,478 ± 0,073	0,426 ± 0,055
ASM	3,174 ± 0,035	4,355 ± 0,182	0,628 ± 0,045	0,496 ± 0,046	0,661 ± 0,042	0,542 ± 0,042
ASM+AF	3,345 ± 0,047	4,277 ± 0,120	0,628 ± 0,045	0,520 ± 0,043	0,646 ± 0,037	**0,555 ± 0,044**
ASM+BF	3,530 ± 0,057	4,265 ± 0,053	0,604 ± 0,047	0,509 ± 0,044	**0,672 ± 0,040**	0,548 ± 0,041
ASM+GF	3,631 ± 0,067	4,289 ± 0,031	0,619 ± 0,044	0,502 ± 0,043	0,668 ± 0,040	0,554 ± 0,043
ASM+IR	4,608 ± 0,121	5,533 ± 0,126	0,649 ± 0,031	0,536 ± 0,040	0,604 ± 0,022	0,521 ± 0,025
ASM+AF+IR	4,838 ± 0,137	5,813 ± 0,057	0,662 ± 0,025	0,561 ± 0,038	0,597 ± 0,023	0,524 ± 0,032
ASM+BF+IR	30,904 ± 1,20	43,640 ± 1,370	0,630 ± 0,041	0,565 ± 0,040	0,585 ± 0,027	0,505 ± 0,025
ASM+GF+IR	5,415 ± 0,187	5,070 ± 0,070	0,636 ± 0,027	0,561 ± 0,038	0,603 ± 0,023	0,521 ± 0,028

Overall results show higher rates for the Median nerve. This may be a consequence of a more uniform anatomic structure of the Median nerve along the arm. Also, between the Cubital nerve and skin exist different anatomical structures that may degenerate the image capture.

Better results can be obtained with the combination of IR images and ASM rather than IR combined with Classical techniques. In contrast to ASM, CT is not fully compatible with IR. Take into account that IR tool increases image resolution and therefore changes its parameters. This may be a drawback since

CT makes use of morphological operations with masks and cuts, which in turn depend on the parameters of the image (i.e. depth and resolution). Thereby, a manual readjustment becomes necessary in order to correct this problem. Nevertheless, it must be noticed that ASM is a supervised method while CT does not require user intervention, it is fully automatic.

4 Conclusions and Future Work

This work presents the HAPAN software supporting the automatic segmentation of peripheral nerves in ultrasound images for developing research, and clinical procedures. The results evidence that HAPAN as an interactive tool allows medical specialists to save time, providing a safer and higher quality process for patient healthcare.

Among the algorithms available in HAPAN, the ASM along with IR yield the best segmentation results thanks to including both supervised and unsupervised information. Particularly, ASM drastically reduces the search area of the nerve structure, thus avoiding undesired structures to appear in the ultrasound image.

As a future work, we plan to develop GPU algorithms to achieve real-time processing. Besides, we will extend the coverage of the database by including additional nerve structures.

Acknowledgments. This work was developed for the research project 111074455958 funded by Colciencias. The authors also acknowledge the electrical engineering master program of Universidad Tecnologica de Pereira for supporting the research project development.

References

1. Chen, S.A., Ong, C.S., Hibino, N., Baschat, A.A., Garcia, J.R., Miller, J.L.: 3D printing of fetal heart using 3D ultrasound imaging data. Ultrasound Obstet. Gynecol. **52**(6), 808–809 (2018)
2. Daoud, M.I., Atallah, A.A., Awwad, F., Al-Najjar, M., Alazrai, R.: Automatic superpixel-based segmentation method for breast ultrasound images. Expert Syst. Appl. **121**, 78–96 (2019)
3. García, H.F., Giraldo, J.J., Álvarez, M.A., Orozco, Á.A., Salazar, D.: Peripheral nerve segmentation using speckle removal and bayesian shape models. In: Paredes, R., Cardoso, J.S., Pardo, X.M. (eds.) IbPRIA 2015. LNCS, vol. 9117, pp. 387–394. Springer, Cham (2015). https://doi.org/10.1007/978-3-319-19390-8_44
4. Giraldo, J.J., Álvarez, M.A., Orozco, Á.A.: Peripheral nerve segmentation using nonparametric Bayesian hierarchical clustering. In: 2015 37th Annual International Conference of the IEEE Engineering in Medicine and Biology Society (EMBC), pp. 3101–3104. IEEE (2015)
5. González, J.G., Álvarez, M.A., Orozco, Á.A.: Automatic segmentation of nerve structures in ultrasound images using graph cuts and Gaussian processes. In: 2015 37th Annual International Conference of the IEEE Engineering in Medicine and Biology Society (EMBC), pp. 3089–3092. IEEE (2015)
6. González, J.G., Álvarez, M.A., Orozco, Á.A.: Peripheral nerves segmentation in ultrasound images using non-linear wavelets and Gaussian processes. In: Paredes, R., Cardoso, J.S., Pardo, X.M. (eds.) IbPRIA 2015. LNCS, vol. 9117, pp. 603–611. Springer, Cham (2015). https://doi.org/10.1007/978-3-319-19390-8_68

7. Illanes, A., Esmaeili, N., Poudel, P., Balakrishnan, S., Friebe, M.: Parametrical modelling for texture characterizationa novel approach applied to ultrasound thyroid segmentation. PloS One **14**(1), e0211215 (2019)
8. Kim, B., Kim, K.C., Park, Y., Kwon, J.Y., Jang, J., Seo, J.K.: Machine-learning-based automatic identification of fetal abdominal circumference from ultrasound images. Physiol. Meas. **39**(10), 105007 (2018)
9. Liu, C., Liu, W., Xing, W.: A weighted edge-based level set method based on multi-local statistical information for noisy image segmentation. J. Vis. Commun. Image Represent. **59**, 89–107 (2019)
10. Ma, L., Kiyomatsu, H., Nakagawa, K., Wang, J., Kobayashi, E., Sakuma, I.: Accurate vessel segmentation in ultrasound images using a local-phase-based snake. Biomed. Sig. Process. Control **43**, 236–243 (2018)
11. Meiburger, K.M., Acharya, U.R., Molinari, F.: Automated localization and segmentation techniques for B-mode ultrasound images: a review. Comput. Biol. Med. **92**, 210–235 (2018)
12. Molinari, F., Caresio, C., Acharya, U.R., Mookiah, M.R.K., Minetto, M.A.: Advances in quantitative muscle ultrasonography using texture analysis of ultrasound images. Ultrasound Med. Biol. **41**(9), 2520–2532 (2015)
13. Moradi, M., Mahdavi, S.S., Guerrero, J., Rohling, R., Salcudean, S.E.: Ultrasound segmentation based on statistical unit-root test of B-scan radial intensity profiles. In: CMBES Proceedings, vol. 33, no. 1 (2018)
14. Nieuwveld, D., Mojica, V., Herrera, A., Pomés, J., Prats, A., Sala-Blanch, X.: Medial approach of ultrasound-guided costoclavicular plexus block and its effects on regional perfussion. Rev. Española de Anestesiología y Reanimación (Engl. Ed.) **64**(4), 198–205 (2017)
15. Smistad, E., Løvstakken, L.: Vessel detection in ultrasound images using deep convolutional neural networks. In: Carneiro, G., et al. (eds.) LABELS/DLMIA -2016. LNCS, vol. 10008, pp. 30–38. Springer, Cham (2016). https://doi.org/10.1007/978-3-319-46976-8_4
16. Srivastava, A., Bhateja, V., Gupta, A., Gupta, A.: Non-local mean filter for suppression of speckle noise in ultrasound images. In: Satapathy, S.C., Bhateja, V., Das, S. (eds.) Smart Intelligent Computing and Applications. SIST, vol. 105, pp. 225–232. Springer, Singapore (2019). https://doi.org/10.1007/978-981-13-1927-3_23
17. Wang, H., Gao, X., Zhang, K., Li, J.: Single-image super-resolution using active-sampling Gaussian process regression. IEEE Trans. Image Process. **25**(2), 935–948 (2016)
18. Wang, W., Li, J., Jiang, Y., Xing, Y., Xu, X.: An automatic energy-based region growing method for ultrasound image segmentation. In: 2015 IEEE International Conference on Image Processing (ICIP), pp. 1553–1557. IEEE (2015)
19. Wieclawek, W., Rudzki, M., Wijata, A., Galinska, M.: Preliminary development of an automatic breast tumour segmentation algorithm from ultrasound volumetric images. In: Pietka, E., Badura, P., Kawa, J., Wieclawek, W. (eds.) ITIB 2018. AISC, vol. 762, pp. 77–88. Springer, Cham (2019). https://doi.org/10.1007/978-3-319-91211-0_7
20. Zhou, Y., Zang, H., Xu, S., He, H., Lu, J., Fang, H.: An iterative speckle filtering algorithm for ultrasound images based on Bayesian nonlocal means filter model. Biomed. Sig. Process. Control **48**, 104–117 (2019)